JOURNAL OF MATERIALS SCIENCE **38** (2003) 2305 – 2310

Fabrication of Li_2O-Al_2O_3-SiO_2 glass-ceramic ferrules by precision drawing of crystallized preforms

A. SAKAMOTO, S. YAMAMOTO
Nippon Electric Glass Co., Ltd., Technical Division, Seiran 2-7-1, Otsu, Shiga 580-8639, Japan
E-mail: asakamoto@neg.co.jp

In this paper, we describe the fabrication of Li_2O-Al_2O_3-SiO_2 (LAS) crystallized preforms with suitable drawing formability, and the characteristics of drawn LAS glass-ceramic capillaries. It was found that addition of K_2O to the LAS glasses reduces crystallinity of the crystallized preforms and forms low-viscosity glass matrices. It was confirmed that, by using a parallel plate viscometer, such crystallized preforms show suitable viscosity for drawing below the melting temperatures of the crystalline phase. We also proved that the addition of K_2O is effective in stabilizing the preforms by preferential precipitation of stable β-spodumene solid solution (s.s.), which is essential in preventing the deposition of coarse surface crystals during the drawing. The LAS glass-ceramic capillaries drawn from the crystallized preform containing 50 mass% β-spodumene s.s. showed a dimensional accuracy within sub-micrometers. It was confirmed that the glass-ceramic capillaries have a low thermal expansion coefficient (25×10^{-7}/K) and excellent mechanical and chemical durability, making them promising candidate components of fiber-optic devices.

1. Introduction

Li_2O-Al_2O_3-SiO_2 (LAS) glass-ceramics exhibit excellent dimension stability due to their small thermal expansion and superb mechanical and chemical durability. Therefore, they seem to be suitable components of fiber-optic devices in which high reliability is required. In fact, they have been used as supporting plates for spliced silica-glass optical fibers [1]. However, the components of most fiber-optic devices are desired to be precisely shaped in the form of rods or capillaries for dimensional fitness to optical fibers. To extend the application of LAS glass-ceramics to such devices, it is essential to establish a highly efficient method for producing precisely shaped rods or capillaries. Machining methods such as grinding or drilling are not effective and are often inapplicable to the production of precisely shaped capillaries. The preform drawing is a sophisticated method for producing precisely shaped glass rods or capillaries as exemplified by the production of optical fibers. This method, however, is inapplicable to the mother glasses of glass-ceramics because of their remarkable crystallizing tendency at high temperature. The mother glasses of glass-ceramics lead to not only undesirable devitrification during drawing but also dimension changes of the products caused by subsequent heat-treatment for crystallization. Thus, the production of precisely shaped glass-ceramics rods or capillaries has not been realized by this method.

We proposed a new method for producing the above-mentioned rods or capillaries which features drawing of the crystallized preforms instead of the mother glass preforms [2]. This method enables the elimination of undesirable devitrification during drawing and subsequent heat-treatment for crystallization. In order to make this method possible, the crystallized preforms must have adequate drawing formability despite the fact that they have been crystallized prior to drawing. Thus, the composition design of the preform materials is an essential issue for the precision drawing of glass-ceramics. Thus far, however, there are no reports regarding fabrication of the crystallized preforms for drawing. In this report, we describe the chemical compositions and the drawing formability of the LAS crystallized preforms for production of precisely shaped LAS glass-ceramic capillaries. First, we studied the composition of LAS glass-ceramics containing a sufficient amount of glass phase to be drawn after the crystallization, and then measured the viscosity of the crystallized specimens using a parallel plate viscometer (PPV) [3, 4]. The drawing formability was investigated by drawing tests, differential thermal analysis (DTA) and powder X-ray diffraction (XRD) analysis. The characteristics of the drawn LAS glass-ceramic capillaries and their applicability to the ferrules used in optical fiber connectors were also discussed.

TABLE I Chemical compositions of glass specimens (mol%)

	A-1	A-2	A-3	A-4	A-5	B-1	B-2	B-3	B-4	C-1	C-2	C-3	D-1	D-2	D-3
SiO_2	73.5	73.7	73.9	74.4	74.5	73.4	72.8	72.0	71.4	71.5	71.4	71.2	74.1	74.0	72.3
Al_2O_3	12.0	12.1	12.2	12.2	12.2	12.2	12.2	12.2	12.2	12.2	12.2	12.2	9.9	9.9	11.8
Li_2O	7.9	6.8	6.1	5.1	4.3	5.1	5.1	5.1	5.1	5.9	6.7	7.7	5.2	5.2	5.2
MgO	1.7	1.7	1.7	1.7	1.7	1.7	1.7	1.7	1.7	1.7	1.7	1.7	1.7	1.7	1.7
TiO_2	2.5	2.5	2.5	2.5	2.5	2.5	2.5	2.5	2.5	2.5	2.5	2.5	2.5	1.5	1.5
ZrO_2	0.9	0.9	0.9	0.9	0.9	0.9	0.9	0.9	0.9	0.9	0.9	0.9	1.0	1.0	0.9
K_2O	0.0	0.0	0.0	0.0	0.0	1.0	1.6	2.4	3.0	2.4	2.4	2.4	2.4	2.4	2.4
ZnO	1.2	1.8	2.2	2.5	3.1	2.5	2.5	2.5	2.5	2.2	1.7	1.2	2.5	2.6	2.5
BaO	0.2	0.3	0.3	0.4	0.5	0.4	0.4	0.4	0.4	0.4	0.3	0.2	0.4	0.7	0.7
CaO	0.0	0.0	0.0	0.0	0.0	0.0	0.0	0.0	0.0	0.0	0.0	0.0	0.0	0.7	0.7
As_2O_3	0.1	0.2	0.2	0.3	0.3	0.3	0.3	0.3	0.3	0.3	0.2	0.1	0.3	0.3	0.3
Total	100.0	100.0	100.0	100.0	100.0	100.0	100.0	100.0	100.0	100.0	100.0	100.0	100.0	100.0	100.0

2. Experimental procedure

The glass compositions used in the experiments are shown in Table I. SiO_2, Al_2O_3, Li_2O and MgO are components of the main crystal, TiO_2 and ZrO_2 are nucleating agents and the others are components that facilitate melting or fining of glasses. All glasses were prepared from mixtures of raw materials including carbonates, nitrates and oxides. The raw materials of industrial grade (purity >99%) were weighed and mixed, then 500 g batches were melted in platinum crucibles at 1600°C for 20 hrs. The molten glass was stirred with a platinum rod at 2 and 15 hrs after finishing batch loading, then poured onto a carbon plate and rolled into 6-mm-thick plates followed by annealing. In order to prepare large preforms for large-scale drawing tests, 20 kg batches were also prepared and melted in a platinum pot under the same conditions with continuous stirring. They were shaped into ingots of 50 mm diameter and 1000 mm length by casting into carbon molds. The glasses were crystallized in electric furnaces. The heat-treatment schedule included a nucleation stage at 780°C for 2 hrs and a crystal-growth stage at 1100°C for 1 hr.

Since LAS glass-ceramics ordinarily have high crystallinity, they show high-temperature resistance and no viscous flow at temperatures below the melting points of the crystalline phase. In order to obtain LAS glass-ceramics with viscous fluidity, we attempted to decrease the crystallinity of a common LAS glass-ceramic A-1, shown in Table I. The crystalline phase and crystallinity were investigated by XRD (Rigaku Rint 2100) analysis. The viscosity of the crystallized glasses was measured with a PPV (Motoyama WRVM-313) using cylindrical specimens with 6 mm diameter and 8 mm length. The drawing tests were carried out by drawing the crystallized rods of 5 mm diameter and 250 mm length into smaller rods of 1 mm diameter using a ring-shaped electric furnace. The loading rate of the specimen into the furnace was 5 mm/min. Large-scale drawing tests were also carried out for some compositions using crystallized preforms with 40 mm outer diameter, 4 mm inner diameter and 900 mm length. The preforms in such dimensions were prepared by grinding the surface of the crystallized ingots, which were formed and crystallized as described above, followed by drilling the center hole using diamond tools. In the drawing, the preform was loaded into the furnace at a rate of 2 mm/min., and was drawn to have an outer diameter of 2.5 mm. The inner diameter of the drawn products was controlled by regulating the pressure in the center hole. In all drawing experiments, the drawing temperatures were determined based on the viscosity of each specimen, in a way that the viscosity was in the range of 10^5 to 10^6 Pa · s at these drawing temperatures. Microstructures of the preforms and the drawn glass-ceramic products were observed by scanning electron microscopy (SEM: JOEL JSM-5400). DTA and measurement of thermal expansion coefficient were carried out using MAC Science TG-DTA 2000 and TD 5000S, respectively.

3. Results and discussion

3.1. Glass-phase formation

In order to confer viscous fluidity to the LAS glass-ceramics, we attempted to increase the amount of glass phase in the glass-ceramics by decreasing the content of Li_2O, which is one of the crystalline phase components in this glass system. The compositions of specimens A-2 to A-5 were decided in such a way that these specimens have less crystallinity than A-1 but have the same residual glass phase composition as A-1, assuming the complete conversion of Li_2O and MgO to β-spodumene s.s. ($Li_2(Mg)O \cdot Al_2O_3 \cdot nSiO_2$; $n \sim 6$), and of TiO_2 and ZrO_2 to the nucleating crystal ($ZrTiO_4$). Fig. 1 shows the relationship between the Li_2O content and the XRD peak intensity observed from crystallized A-1 to A-5. The amount of β-spodumene s.s. decreases

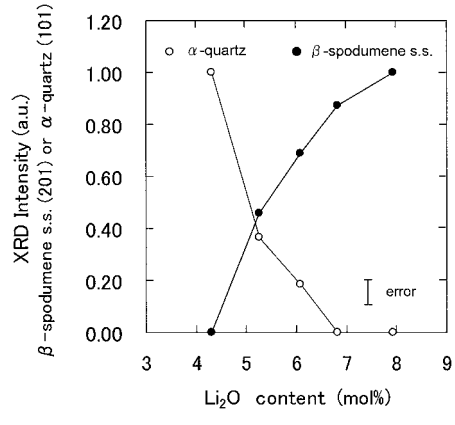

Figure 1 X-ray diffraction peak intensity of crystallized specimens with various Li_2O contents. Lines between each dot were drawn to show tendencies.

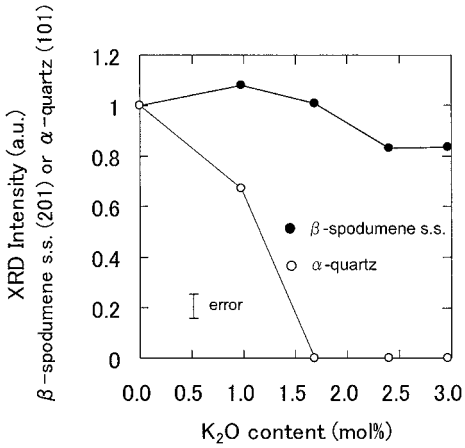

Figure 2 X-ray diffraction peak intensity of crystallized specimens with 5.1 mol% Li_2O and various K_2O contents. Lines between each dot were drawn to show tendencies.

with decreasing Li_2O content, whereas α-quartz starts to precipitate, being the main crystal at 4.3 mol% Li_2O. The precipitation of α-quartz inhibits not only the glass-phase formation but also the small thermal expansion of the glass-ceramics. Thus, it was found that the Li_2O content cannot be reduced to less than 6.8 mol%, unless the precipitation of α-quartz is prevented.

According to the study of Kracek [5], the liquidus temperature of SiO_2 family crystals in SiO_2-R_2O (R: alkali ions) glasses decreases with increasing R_2O content, and K_2O has the most remarkable effect. Assuming that K_2O plays the same role in the LAS system, we attempted to suppress the precipitation of α-quartz in A-4 by substituting K_2O for SiO_2 (specimens B-1 to B-4). Fig. 2 shows the XRD peak intensity of α-quartz (101) and β-spodumene s.s. (201), plotted against the K_2O content. It is evident from the figure that the precipitation of α-quartz is selectively suppressed by the addition of K_2O, whereas the amounts of β-spodumene s.s., which exhibits small thermal expansion, are almost constant. A K_2O content higher than 1.7 mol% resulted in a crystalline phase consisting of only β-spodumene s.s. The XRD peak intensities of β-spodumene s.s. precipitated in the specimens containing 2.4 mol% K_2O (B-3 and C-1 to C-3) are shown in Fig. 3 for various Li_2O contents. The results for A-1 and A-2 without K_2O are also plotted for comparison. The intensity of

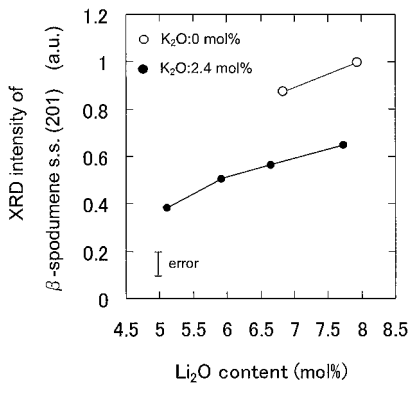

Figure 3 X-ray diffraction peak intensity of β-spodumene s.s. (201) in specimens with various Li_2O and K_2O contents. Lines between each dot were drawn to show tendencies.

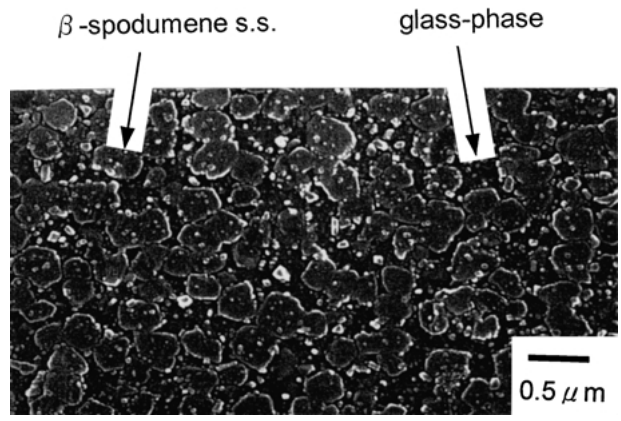

Figure 4 Scanning electron micrograph of the bulk structure of crystallized specimen with B-3 composition.

the specimens with K_2O decreases to about 2/3 of that of the specimens without K_2O, and gradually decreases with decreasing Li_2O content. These results indicate that the addition of K_2O is effective in both preferential precipitation of β-spodumene s.s. and the glass-phase formation, and furthermore that the amount of the glass phase can be controlled by Li_2O content. The bulk structure of crystallized B-3 is shown in Fig. 4. The figure shows that the crystalline phase of β-spodumene s.s. with a grain size of about 0.3 μm coexists with the glass phase which surrounds each crystal grain.

3.2. Viscosity after crystallization

In order to evaluate the viscous fluidity of the crystallized specimens, their viscosity was measured by PPV. The cylindrical specimens were subjected to indentation by a metal spike or to pressing by a pair of parallel metal plates with increasing temperature [4]. The results for specimens with 2.4 mol% K_2O (B-3 and C-3) and specimens without K_2O (A-1 and A-4) are shown in Fig. 5. The arrows in the figure indicate the melting temperatures of the crystalline phase of each specimen, which were determined by DTA. The slopes of the viscosity curves for A-1 and A-4 are steeper than those for

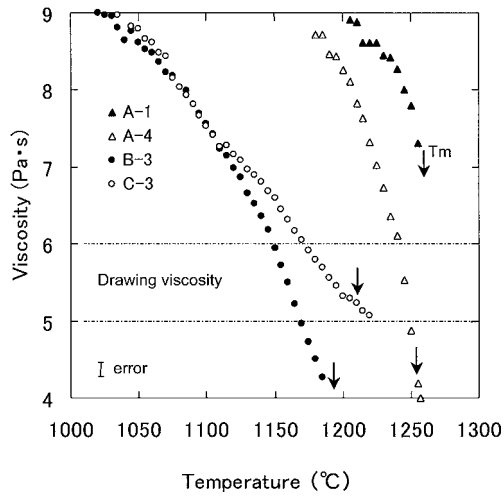

Figure 5 Viscosity of crystallized specimens. Each arrow shows the melting temperature of the crystalline phase (Tm) in the corresponding specimen.

B-3 and C-3, and the temperature range for achieving the drawing viscosity (10^5 to 10^6 Pa · s) is very close to the melting temperatures of the crystalline phase. This suggests that the decreases in viscosity of A-1 and A-4 in this temperature range are caused by the melting of the crystalline phases. Thus, the drawing of such preforms cannot maintain the crystalline phases in the drawn products. On the other hand, in the case of B-3 and C-3, they show lower viscosity than A-1 and A-4, and less steep viscosity curves, providing considerably lower drawing temperatures than the melting temperatures of their crystalline phases. It is evident that the viscosity behavior of these specimens is due to the viscous flow of the glass phase including K_2O existing around the crystal grains, as shown in Fig. 4. It is probable that such glass-ceramics can be drawn at temperatures below the melting points without marked changes in their crystalline phases. The drawing formability of such crystallized preforms will be discussed in the next section.

3.3. Drawing formability

The drawing tests were carried out using the crystallized specimens with the diameters of 5 mm, which are listed in Table II. In addition to B-3 and C-3 mentioned above, D-1 and D-2 with different crystalline phase constitutions were also tested. The amounts of glass phases shown in the table were determined by crystallinity measurement using XRD analysis [6] with ±5 mass% accuracy. D-1 has a mixed crystalline phase with 30 mass% β-spodumene s.s. and 20 mass% α-quartz, and the crystalline phase of D-2 consists of β-quartz s.s. D-3, which has a similar composition to D-2 but has a different crystalline phase, β-spodumene s.s., was also prepared. All specimens were drawn under the same conditions except for the drawing temperature. The drawing temperatures were listed in Table II. They were determined based on the viscosity of each specimen, in a way that the specimens show the viscosity between 10^5 to 10^6 Pa · s at these temperature. The crystalline phase of all specimens after drawing consisted of only β-spodumene s.s. As shown in Table II, B-3, C-3 and D-3 showed good drawing formability, whereas D-1 and D-2 yielded frail products with coarse surface crystals. The typical appearances of the drawn products are exemplified by those of D-2 and D-3, as shown in Fig. 6. It can easily be seen that D-3 has a smooth surface, on the contrary, D-2 has coarse crystals

TABLE II Specimens for drawing tests and their drawing formability

Specimen	Glass phase (mass%)	Drawing temp. (°C)	Crystalline phase: Before drawing	Crystalline phase: After drawing	Formability
B-3	50	1170	β-spd	β-spd	Good
C-3	40	1170	β-spd	β-spd	Good
D-3	50	1150	β-spd	β-spd	Good
D-1	50	1150	β-spd +α-q	β-spd	Broken, coarse surface crysta
D-2	55	1130	β-q	β-spd	Broken, coarse surface crystal

β-spd: β-spodumene s.s., α-q: α-quartz , β-q: β-quartz s.s.

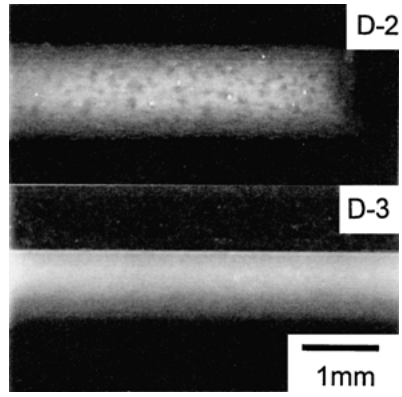

Figure 6 Typical appearance of drawn products surface.

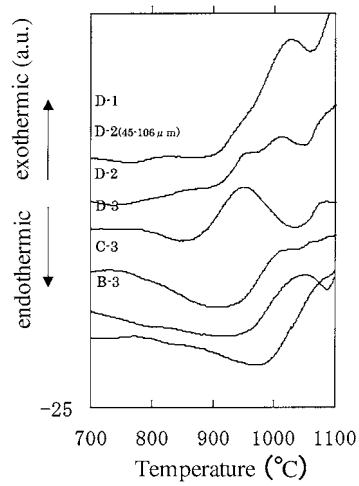

Figure 7 Differential thermal analysis curves obtained from crystallized specimen powders.

deposited on its surface, resulting in deteriorated products.

In order to investigate the cause of the large difference in drawing formability among these specimens, their thermal stability was studied by DTA. Each specimen was crystallized prior to the DTA under the prescribed conditions, then powdered to grain sizes smaller than 45 μm. D-2 with larger grain sizes (45 to 106 μm) was also subjected to the analysis. Fig. 7 shows the DTA results of the specimens listed in Table II, indicating that the curves can be classified into two groups: the curves including pseudo-endothermic peaks due to sintering of the specimens (B-3, C-3 and D-3), and the curves including exothermic peaks (D-1 and D-2). All exothermic peaks were located at temperatures lower than the crystallization temperature (1100°C). In the case of D-2, however, the exothermic peak shifted towards higher temperatures when the specimen has a larger grain size. These phenomena are characteristic of surface crystallization. Furthermore, the two groups mentioned above were found to be in good agreement with the drawing test results, that is, the endothermic group showed good drawing formability, but the exothermic group showed coarse crystal deposition. Table III shows the crystalline species before and after the DTA. The crystalline phases after the DTA consisted of only β-spodumene s.s., which is in good agreement with the drawing test results. It was also found that, in the case of

TABLE III Crystalline phase changes during DTA

DTA curve	Sample no.	Crystalline phase		I/I_0
		Before DTA	After DTA	
Endothermic	B-3	β-spd	β-spd	0.98
	C-3	β-spd	β-spd	0.99
	D-3	β-spd	β-spd	0.94
Exothermic	D-1	β-spd + α-q	β-spd	1.27
	D-2	β-q	β-spd	∞

β-spd: β-spodumene s.s., α-q: α-quartz, β-q: β-quartz s.s.
I/I_0: XRD intensity ratio of β-spodumene s.s. (201). I_0: before DTA, I: after DTA.

the endothermic group, there was no significant change in the XRD peak intensity of β-spodumene s.s. (201) before and after the DTA, whereas the exothermic group showed the transformation of the crystalline species to β-spodumene s.s. after the DTA, and the corresponding changes in the peak intensity. These findings indicate that the exothermic peaks in Fig. 7 correspond to the transformation of crystalline species from α-quartz or β-quartz s.s. to β-spodumene s.s. induced by surface crystallization. Surface crystallization often arises from the increase in specific surface area of the specimens that are thermodynamically unstable, as exemplified by the exothermic peaks in DTA. Thus, if such preforms that show the exothermic peaks in DTA are drawn, the rapid increase in their specific surface area will cause surface crystallization leading to phase transformation or further crystallization, and eventually to the deposition of coarse crystals on their surface. As for D-1 and D-2, since they contain α-quartz or β-quartz s.s., the crystalline phases may tend to transform to the stable β-spodumene s.s. during drawing. Thus, one can say that, in order to achieve precision drawing of crystallized preforms, it is essential to prepare stable preforms with less surface crystallization tendency, excluding the metastable crystalline phases. It was also demonstrated that the drawing formability of the preforms can be predicted through the surface crystallization tendency using DTA.

3.4. Characteristics of LAS glass-ceramic capillaries

Precise LAS glass-ceramic capillaries (GCCs) were produced through large-scale drawing at 1160°C using the stable crystallized preform with B-3 composition, which involves 50 mass% β-spodumene s.s. The large-scale cylindrical preform with the outer diameter of 40 mm was used as described above. Fig. 8 shows the neck-down portion of the crystallized preform after drawing and cross-section of the capillaries. It can be seen from the figure that the crystallized preform deformed into a symmetrical cone shape, and the GCC has a dimensional accuracy within sub-micrometers. The crystalline phase of the capillaries was β-spodumene s.s. with 40 mass% crystallinity. This indicates that most part of the crystalline phase was maintained during drawing without a significant decrease in crystallinity. Since the GCC has already been crystallized, there is no need for heat-treatment for further crystallization. Therefore, the accurate dimensions of the GCC shown in Fig. 8 are available for the final products as they are. A SEM image of the GCC surface is shown in Fig. 9. It can be seen that fine crystals are distributed in the glass matrix. The surface roughness of the GCC was 0.2 μm (Ry). The GCC showed a thermal expansion coefficient of 25×10^{-7}/K between 30 to 300°C, which was smaller than that of general heat-resistant glasses, and a high bending strength of 700 MPa. These figures did not change even after exposure to 85°C and 90% RH for 1500 hrs.

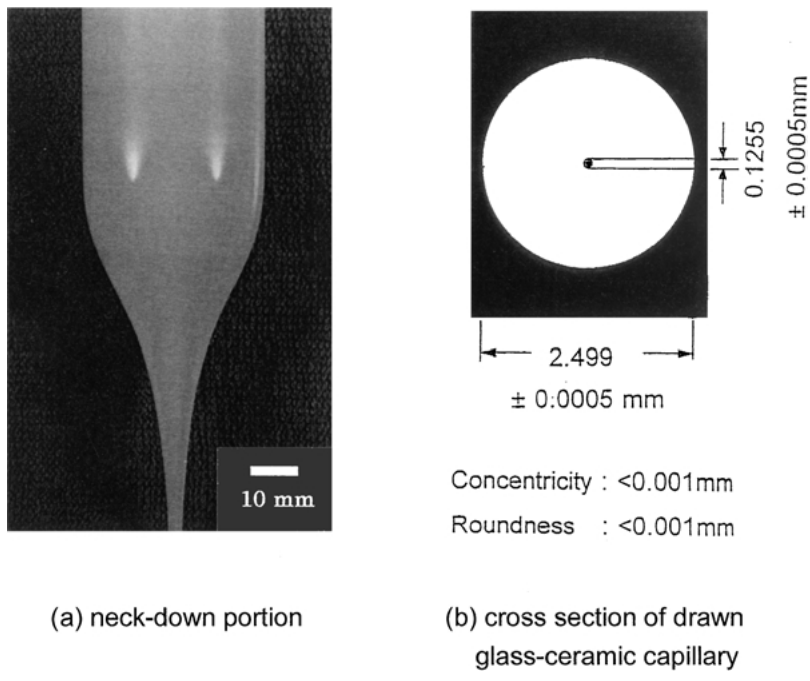

Figure 8 The neck-down portion of the drawn crystallized preform with B-3 composition (a). A cross-sectional view of the drawn glass-ceramic capillary (b).

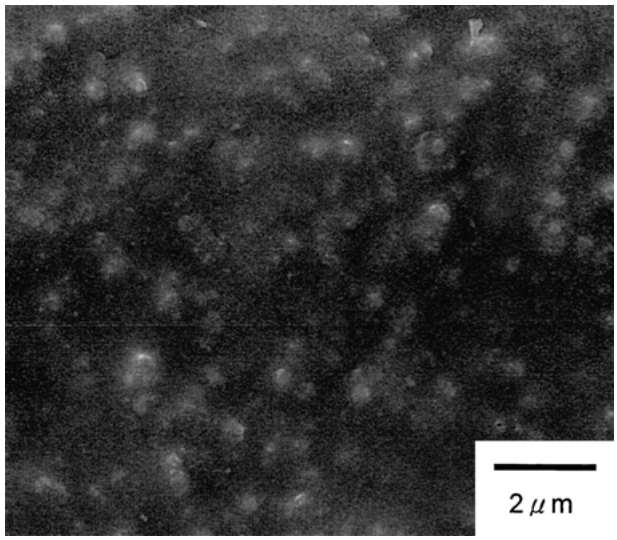

Figure 9 Scanning electron micrograph of the surface of the drawn glass-ceramic capillary with B-3 composition.

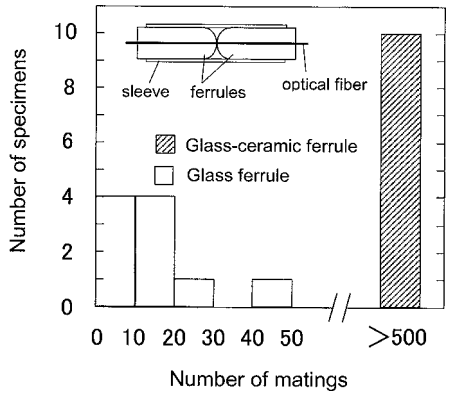

Figure 10 Results of scratch resistance tests of glass-ceramic ferrules and non-crystalline glass ferrules. Inset: Assembly of ferrules for mating.

There are some reports concerning the potential application of glass-ceramics to ferrules used in optical fiber connectors [2, 7–9]. Ferrules are composed of high-precision capillaries, and used for the alignment of optical fibers. The GCC having excellent dimension accuracy and the properties mentioned above appear to be suitable for ferrule applications. The inset of Fig. 10 shows a representative use of the GCC. The optical signal delivered by a fiber could be efficiently coupled to another one by placing a pair of GCCs in a zirconia alignment sleeve [10]. Since ferrules are mated many times in the alignment sleeves, they should have good scratch resistance against repeated mating. Fig. 10 shows the results of scratch resistance tests for the ferrules made of GCC. Each specimen was repeatedly mated in the zirconia sleeve, and their surface was observed under an optical microscope after every 10 matings. The numbers on the abscissa of the figure indicate the maximum mating times after which the ferrules were maintained without scratching, and the ordinate indicates the numbers of the specimens. The results of boro-silicate glass ferrules are also shown for comparison. It was found that ferrules made of GCC can withstand more than 500 matings without scratching, indicating their great superiority over glass ferrules. In general, crystals are harder than glasses, and crystal grain boundaries in the glass-ceramics interfere with crack propagation. Therefore, the excellent scratch resistance of GCC is explained by the presence of numerous fine crystals on the GCC surface as shown in Fig. 9.

4. Conclusion

The chemical compositions of the LAS glass-ceramics suitable for the precision drawing of crystallized preforms were developed. We succeeded in controlling the crystallinity by depression of the precipitation of α-quartz with no interference in the precipitation of β-spodumene s.s. by addition of K_2O. Since the precipitation of α-quartz was effectively depressed, a suitable viscous fluidity of the crystallized preforms was achieved, thus, precision drawing at temperatures below the melting point of β-spodumene s.s. crystalline phase has been realized. Furthermore, the deposition of coarse surface crystals during such drawing was suppressed in these new compositions. It was also confirmed that LAS glass-ceramic capillaries drawn from a crystallized preform have excellent dimensional accuracy within sub-micrometers, small thermal expansion, large bending strength, high-temperature humid-environment durability and outstanding scratch resistance, indicating their potential use for ferrules in optical fiber connectors.

Acknowledgement

Careful reading of the manuscript by Dr. Junji Nishii of National Institute of Advanced Industrial Science and Technology is greatly appreciated.

References

1. A. SAKAMOTO and T. SHIBUYA, Japanese Patent No. 2017703.
2. A. SAKAMOTO, M. WADA, H. TAKEUCHI and M. NINOMIYA, in Proceedings of the 18th International Congress on Glass, San Francisco, July 1998, Vol. C6, p. 62.
3. E. H. FONTANA, *Ceramic Bulletin* **49**(6) (1970) 594.
4. Y. SHIRAISHI, S. NAGASAKI and M. YAMASHIRO, *J. Japan Inst. Metals* **60**(2) (1996) 184.
5. F. C. KRACEK, *J. Amer. Chem. Soc.* **52**(4) (1930) 1440.
6. L. E. ALEXANDER, "X-ray Diffraction Methods in Polymer Science," Japanese edn. (Kagaku Dojin, Kyoto, 1973) p. 126.
7. R. NAGASE, Y. TAKEUCHI and S. MITACHI, *Electr. Lett.* **33**(14) (1997) 1243.
8. Y. TAKEUCHI, S. MITACHI and R. NAGASE, *IEEE Photonics Tech. Letters* **9**(11) (1997) 1502.
9. S. MITACHI, R. NAGASE, Y. TAKEUCHI and R. HONDA, *Glass Technol.* **39**(3) (1998) 98.
10. E. SUGITA, R. NAGASE, K. KANAYAMA and T. SHINTAKU, *J. Lightwave Tecnol.* **7**(11) (1989) 1689.

Received 26 August 2002
and accepted 29 January 2003